Supplementary Information for

Diethylenetriamine functionalized magnetic chitosan/magnetic polyglycidyl methacrylate for Pb(II), Cd(II), and Cu(II) recovery from water

Huda M. Alghamdi[1], Ahmed M. Elgarahy[2], Khalid Z. Elwakeel[1*]

[1]University of Jeddah, College of Science, Department of Chemistry, Jeddah, Saudi Arabia.

[2]Environmental Chemistry Division, Environmental Science Department, Faculty of Science, Port Said University, Port Said, Egypt.

Author	E-mail	ORCID number
Huda M. Alghamdi	halghamdi3@uj.edu.sa	0009-0009-3091-7024
Ahmed M. Elgarahy	ahmed.gamal@sci.psu.edu.eg	0000-0003-4959-2652
Khalid Z. Elwakeel	kelwkeel@uj.edu.sa	0000-0002-8853-284X

∗Corresponding author: University of Jeddah, College of Science, Department of Chemistry, Jeddah, Saudi Arabia.; kelwkeel@uj.edu.sa (K. Z. Elwakeel).

1. Synthesis of Fe_3O_4 nanoparticles

Magnetite (Fe_3O_4) nanoparticles were synthesized via hydrothermal co-precipitation of ferric and ferrous salts, following the method reported by Elwakeel et al. (2020).[1] Briefly, ferrous sulfate heptahydrate ($FeSO_4 \cdot 7H_2O$, 5.0 g) and ammonium iron(III) sulfate dodecahydrate ($(NH_4)Fe(SO_4)_2 \cdot 12H_2O$, 17.35 g) were dissolved in deionized water (250 mL). The solution was heated to 333 ± 1 K under a nitrogen atmosphere with continuous magnetic stirring for 60 min. Aqueous NaOH (3 M) was then added dropwise until pH 12 was attained, and the reaction proceeded for an additional 5 h at 318 K. The resulting Fe_3O_4 nanoparticles were magnetically separated, repeatedly washed with Milli-Q water (Millipore, Billerica, MA, USA) until neutral pH was achieved, rinsed with acetone, and vacuum-dried at 333 ± 1 K for 5 h.

Table S1: Some physicochemical properties of cadmium, copper, and lead[2]

Parameter	Cu(II)	Cd(II)	Pb(II)
Atomic radius (pm)	128	149	175
Covalent radius (pm)	117	141	154
Divalent ion radius (pm)	72	97	120
Hydration heat (kJ/mol)	83	373	697
Ion charge density[a]	6.2517	5.3718	1.7059
Standard electrode potential (V)	-0.762	-0.4029	-0.1263

Table S2: Kinetics models

Kinetics model	Equation	References
Pseudo-First order	$q_t = q_{e(th)}\left(1 - e^{-k_1 t}\right)$	3
Pseudo-Second order	$q_t = \frac{k_2 q_{e(th)}^2 t}{1 + k_2 q_{e(th)} t}$	4
Intraparticle diffusion	$q_{t = k_i + X}$	5
Elovich equation	$\frac{dq_t}{dt} = \alpha e^{-\beta q_t}$	6

q_t (mg g^{-1}): amount of metal ion sorbed at time (t).

$q_{e(th)}$ (mg g^{-1}): equilibrium sorption.

K_1 (min^{-1}): pseudo first -order rate constant of adsorption.

K_2 (g mg^{-1} min^{-1}): pseudo second-order rate constant of adsorption.

K_i (mg g^{-1} min$^{-0.5}$): the intra-particle diffusion rate.

X (mg g^{-1}): the boundary layer diffusion effects (external film resistance).

α (mg g^{-1} min^{-1}): the initial sorption rate.

β (g mg^{-1}): the desorption constant.

Table S3: Sorption isotherms

Isotherm	Equation	References
Langmuir	$q_e = \frac{K_L q_m C_e}{1 + K_L C_e}$	[7]
Freundlich	$q_e = K_F C_e^{1/n}$	[8]
Temkin	$q_e = \frac{RT}{b_T} \ln\left(K_T C_e\right)$	[9]

C_e (mg L^{-1}): equilibrium concentration of metal ion in solution.

q_e (mg g^{-1}): amount of dye sorbed at equilibrium.

q_m (mg g^{-1}): Langmuir maximum sorption capacity.

K_L (L mg^{-1}): Langmuir constant related to affinity of sorptive sites.

K_f (mg g^{-1}) (L $mmol^{-1})^{1/n}$: Freundlich constant relative sorption capacity.

n: Freundlich constants related to the sorption capacity and intensity

K_T (L g^{-1}): Temkin constant.

B_T (kJ mg^{-1}): Temkin constant.

Table S4: Chemical analysis of water samples collected from a drinking water supply facility in Port-Said, Egypt

Parameter	**Unit**	**Result**	**Parameter**	**Unit**	**Result**
Temperature	°C	24	NH_3-N	ppm	0.03
Turbidity	NTU	0.5	NO_2-N	ppm	0.004
PH	-	7.1	NO_3-N	ppm	0.9
TDS	ppm	514	PO_4-P	ppm	0.1
Total Hardness	ppm	174	Fe	ppm	0.04
Ca Hardness	ppm	111	Mn	ppm	0.032
Mg Hardness	ppm	63	Cu	ppm	0.01
Cl	ppm	93	Zn	ppm	0.03
Alkalinity	ppm	141	Al	ppm	0.121
SO_4	ppm	171	Total bacterial count	CFU/ml	2

Table S5: Chemical analysis of wastewater sample collected from petrochemical plant discharge, Port Said, Egypt

Parameter	Unit	Result
Conductivity	µS/cm	11240
TDS	ppm	7530
PH	-	7.84
Total hardness	ppm	1131
Alkalinity	ppm	97
Iron	ppm	0.28
Turbidity	NTU	2.8
Ammonia	ppm	0.8
TSS	ppm	15.4

Table S6: Comparison of sorption performance for Pb(II) with various sorbents in the present and other studies

Adsorbent	**Sorption capacity (mg g^{-1})**	**References**
Porous Carbon nanofibers	7.1	[10]
Untreated Biochar	7.57	[11]
HCl deashed Biochar	9.77	[11]
HF deashed Biochar	16.70	[11]
Activated Potassium acetate biochar	38.49	[11]
Mesoporous coral limestones	39.26	[12]
Activated Potassium acetate - HCl deashed Biochar	40.39	[11]
Iron hydroxyphosphate composites	43.203	[13]
Magnetic cellulose acetate	44	[14]
The ion-imprinted and CNF-grafted polymeric beads	47.62	[15]
Activated Potassium acetate - HF deashed Biochar	49.47	[11]
Phosphorus rich biochar	62	[16]
Diethylenetriamine/magnetic chitosan/glycidyl methacrylate composite	70.42	Present study

Table S7: Comparison of sorption performance for Cd(II) with various sorbents in the present and other studies

Adsorbent	**Sorption (mg g^{-1})**	**References**
Light-restricted *C. vulgaris*	8.0	[17]
Cyanobacterium of Aphanothece sp cultivar based adsorbent	8.20	[18]
Deposited silt	10.25	[19]
Nitrogen-restricted *C. vulgaris*	11.9	[17]
Raw vermiculite (VER)	14.98	[20]
Dodecyl dimethyl betaine modified vermiculite (BS-VER)	16.03	[20]
Potassium permanganate activated black seeds (KMBS)	19.79	[21]
Nanoscale zero-valent iron - zeolite composite	20.6	[22]
Natural Jordanian (NJ) zeolite	25.9	[23]
Diethylenetriamine/magnetic chitosan/glycidyl methacrylate composite	59.17	Present study

Table S8: Comparison of sorption performance for Cu(II) with various sorbents in the present and other studies

Adsorbent	**Sorption capacity ($mg\ g^{-1}$)**	**References**
Manganese oxide (MnO_2) nanowires	2.972	[24]
Activated carbon derived from modified rice husk	3.85	[25]
Magnetic activated carbon derived from modified rice husk	4.52	[25]
C-phenylcalix[4]pyrogallolarene	8.14	[26]
Ceramsite	9.42	[27]
Granular activated carbon-magnetite nanoparticles composite	13.37	[28]
Granular Activated Carbon-Supported Titanium Dioxide Particles	23.42	[29]
Powdered activated carbon-magnetite nanoparticles composite	23.61	[28]
Histidine modified montmorillonite	30.72	[30]
Diethylenetriaminepentaacetic acid-chitosan sewage sludge composite	31.42	[31]
Polyethylenimine modified wheat straw	48.6	[32]
Diethylenetriamine/magnetic chitosan/glycidyl methacrylate composite	55.24	Present study

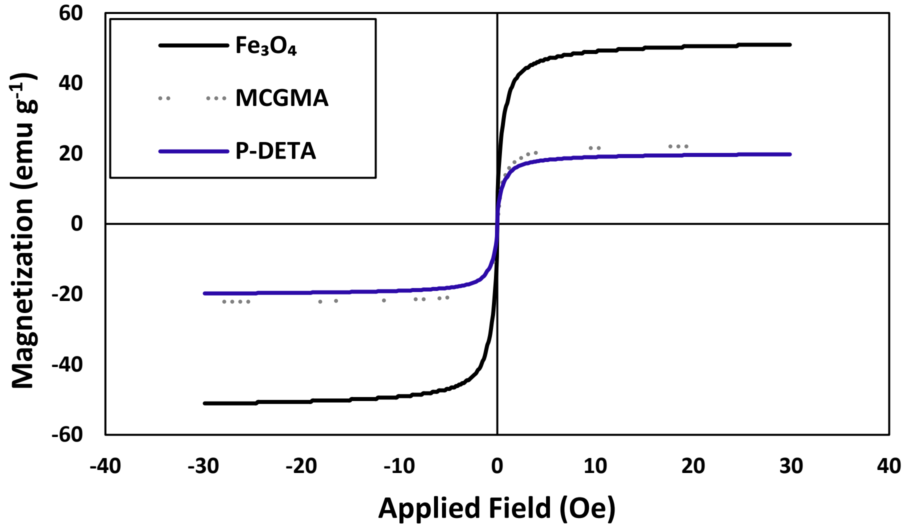

(a)

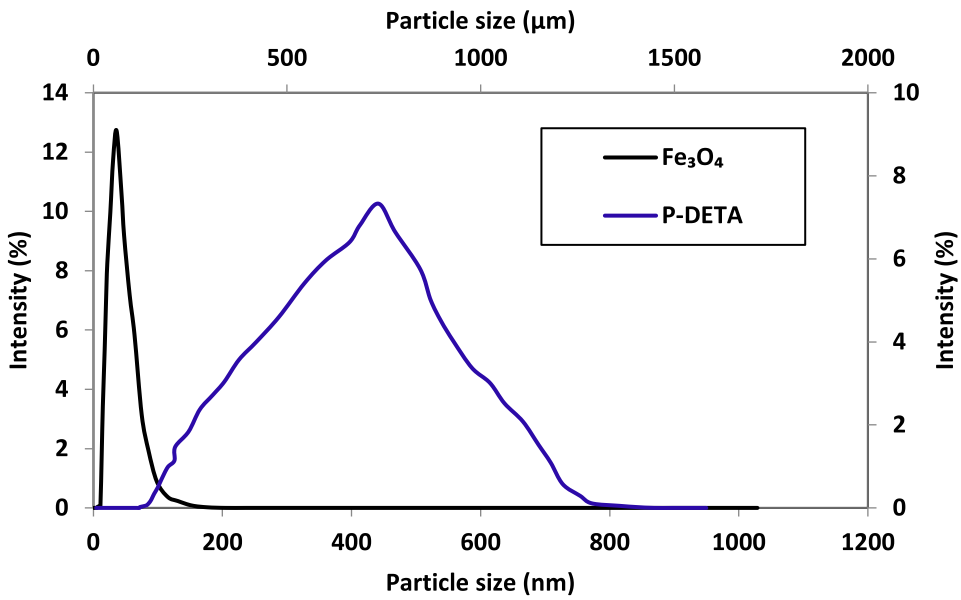

(b)

Figure S1: (a) Magnetic hysteresis loops of Fe_3O_4, MCGMA, and P-DETA composites measured at room temperature, showing the variation in magnetization (emu g^{-1}) as a function of the applied magnetic field (Oe); (b) Particle size distribution profiles of Fe_3O_4 and P-DETA materials obtained by dynamic light scattering (DLS).

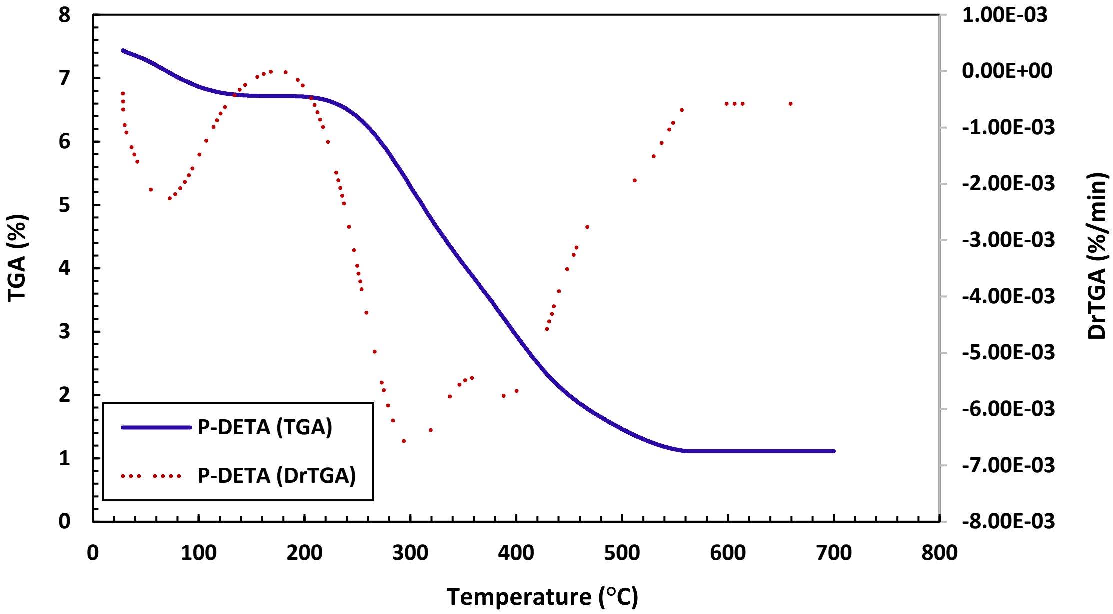

Figure S2: Thermogravimetric analysis (TGA) and derivative thermogravimetry (DTG) curves of P-DETA. The TGA curve (solid blue line) shows the percentage weight loss as a function of temperature, indicating distinct decomposition steps, while the DTG curve (dotted red line) reveals the corresponding rate of weight loss.

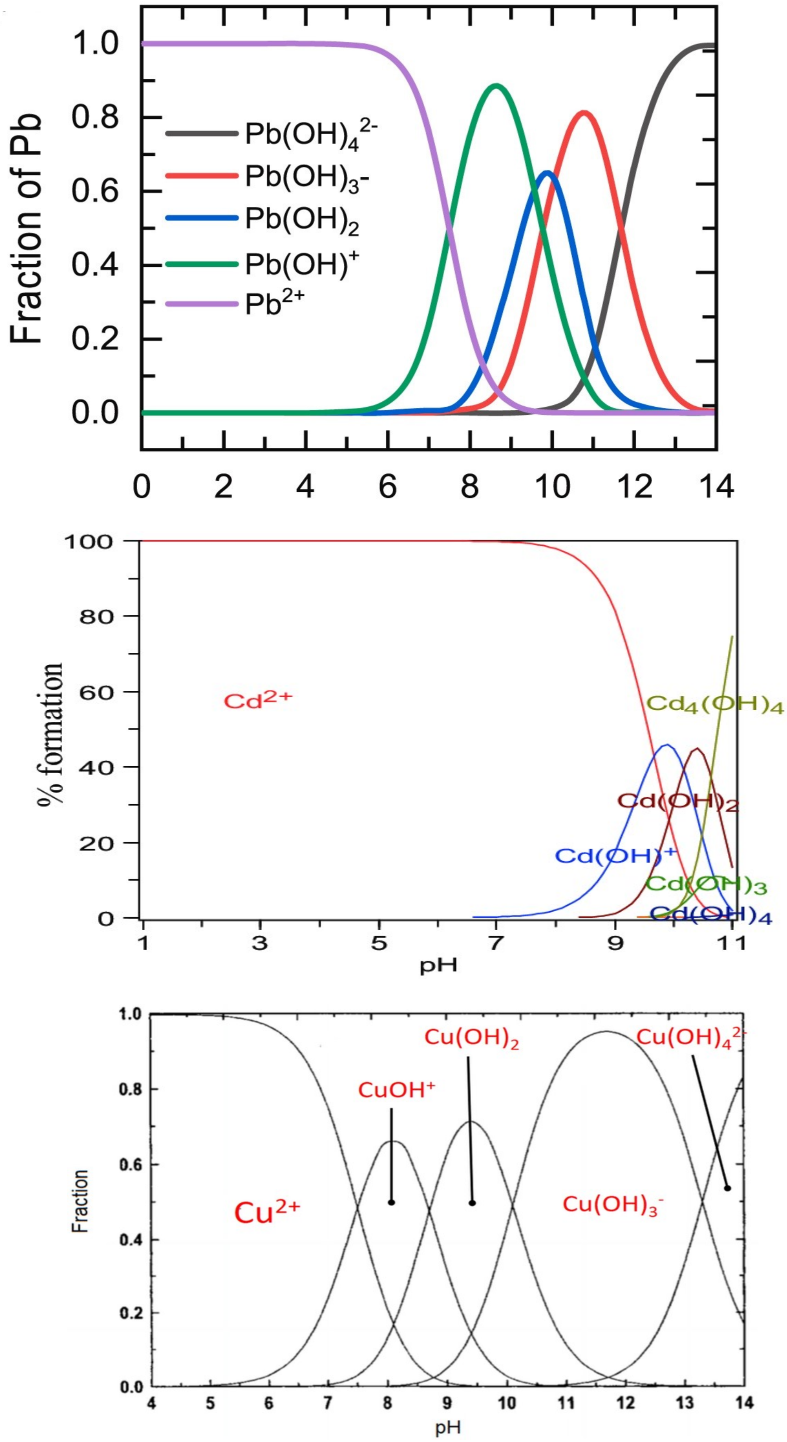

Figure S3: Speciation diagrams of Pb(II), Cd(II), and Cu(II) ions as a function of pH; (a) Lead (Pb) species distribution showing predominant presence of Pb^{2+} at low pH, and successive formation of hydrolyzed species $Pb(OH)^{+}$, $Pb(OH)_2$, $Pb(OH)_3^{-}$, and $Pb(OH)_4^{2-}$ with increasing pH [33]; (b) Cadmium (Cd) species distribution, where Cd^{2+} dominates at pH < 8, followed by the gradual appearance of $Cd(OH)^{+}$, $Cd(OH)_2$, and polynuclear complexes such as $Cd_4(OH)_4$ and $Cd(OH)_4^{2-}$ at higher pH [34]; (c) Copper (Cu) species distribution illustrating the prevalence of Cu^{2+} under acidic conditions, and formation of $CuOH^{+}$, $Cu(OH)_2$, $Cu(OH)_3^{-}$, and $Cu(OH)_4^{2-}$ in more alkaline media [35].

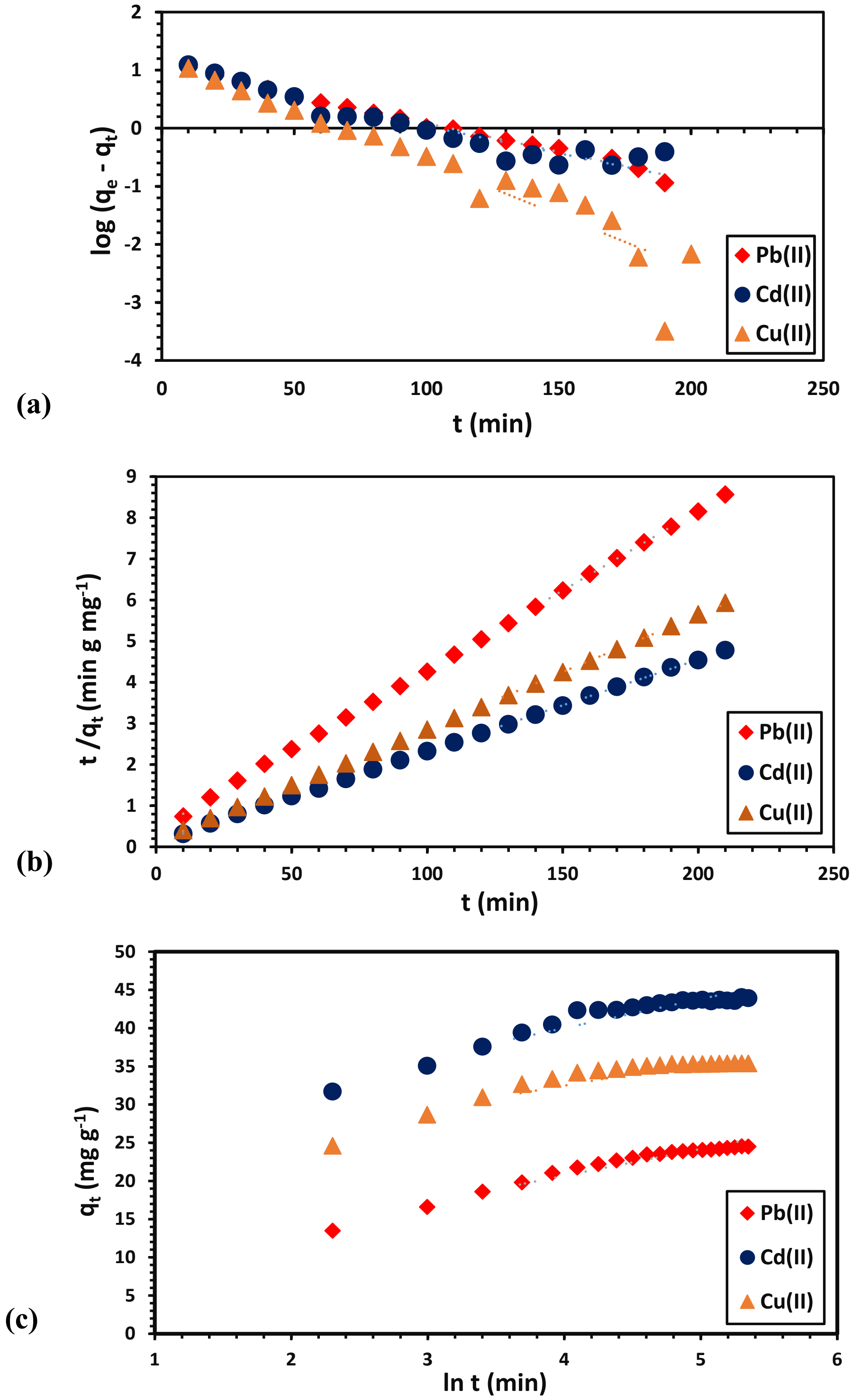

Figure S4: Kinetic modeling of Pb(II), Cd(II), and Cu(II) adsorption onto the adsorbent surface using three linearized models; (a) Pseudo-first-order model: Plot of $\log(q_e - q_t)$ versus time (t); (b) Pseudo-second-order model: Plot of t/q_t versus time (t); (c) Intraparticle diffusion model: Plot of q_t versus ln(t).

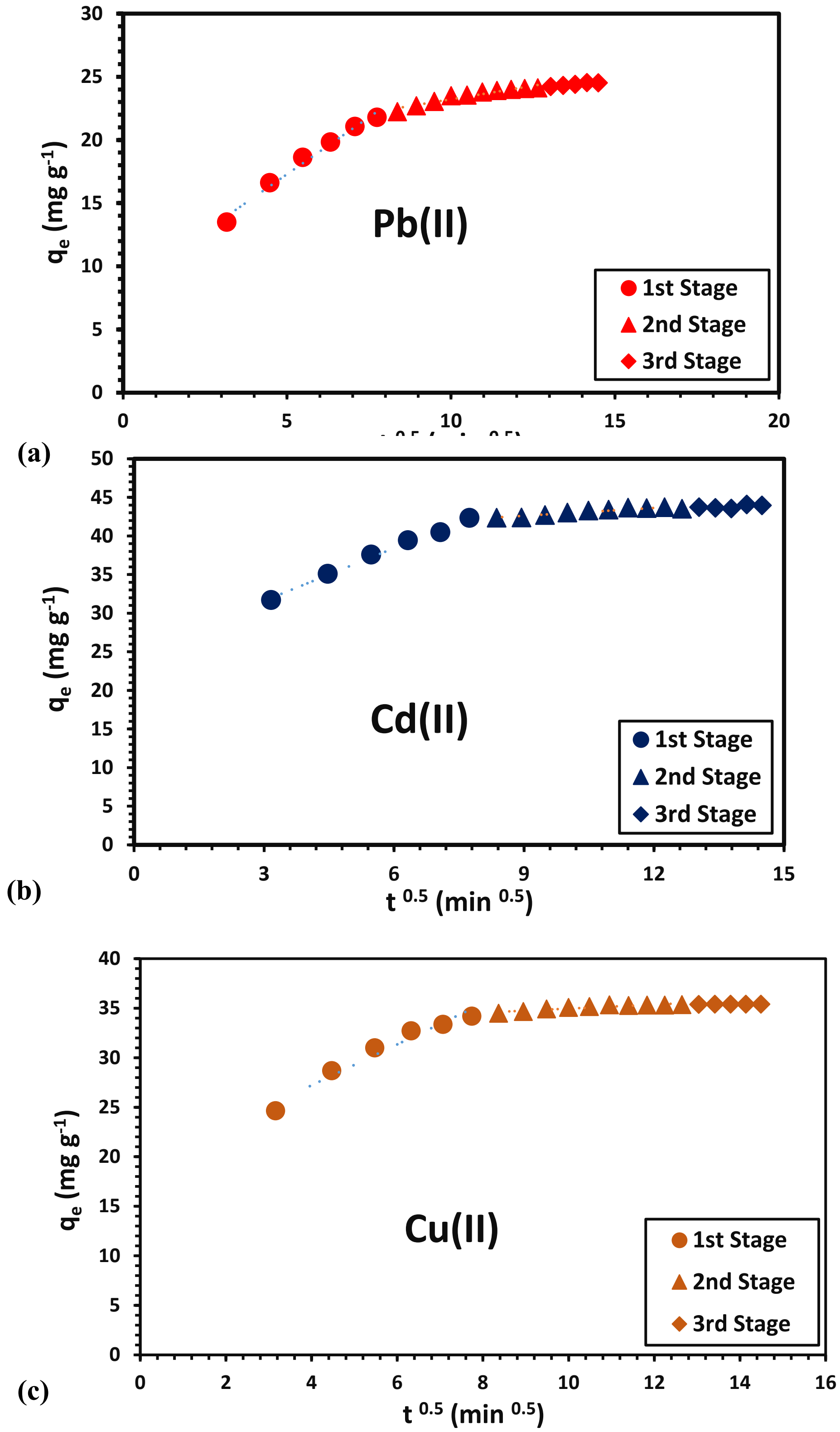

Figure S5: Intraparticle diffusion model plots showing the multi-stage adsorption kinetics of (a) Pb(II), (b) Cd(II), and (c) Cu(II) ions onto the adsorbent. The plots reveal three distinct linear regions corresponding to different adsorption phases:1st stage – rapid external surface adsorption, 2nd stage – gradual intraparticle diffusion, and 3rd stage – equilibrium phase.

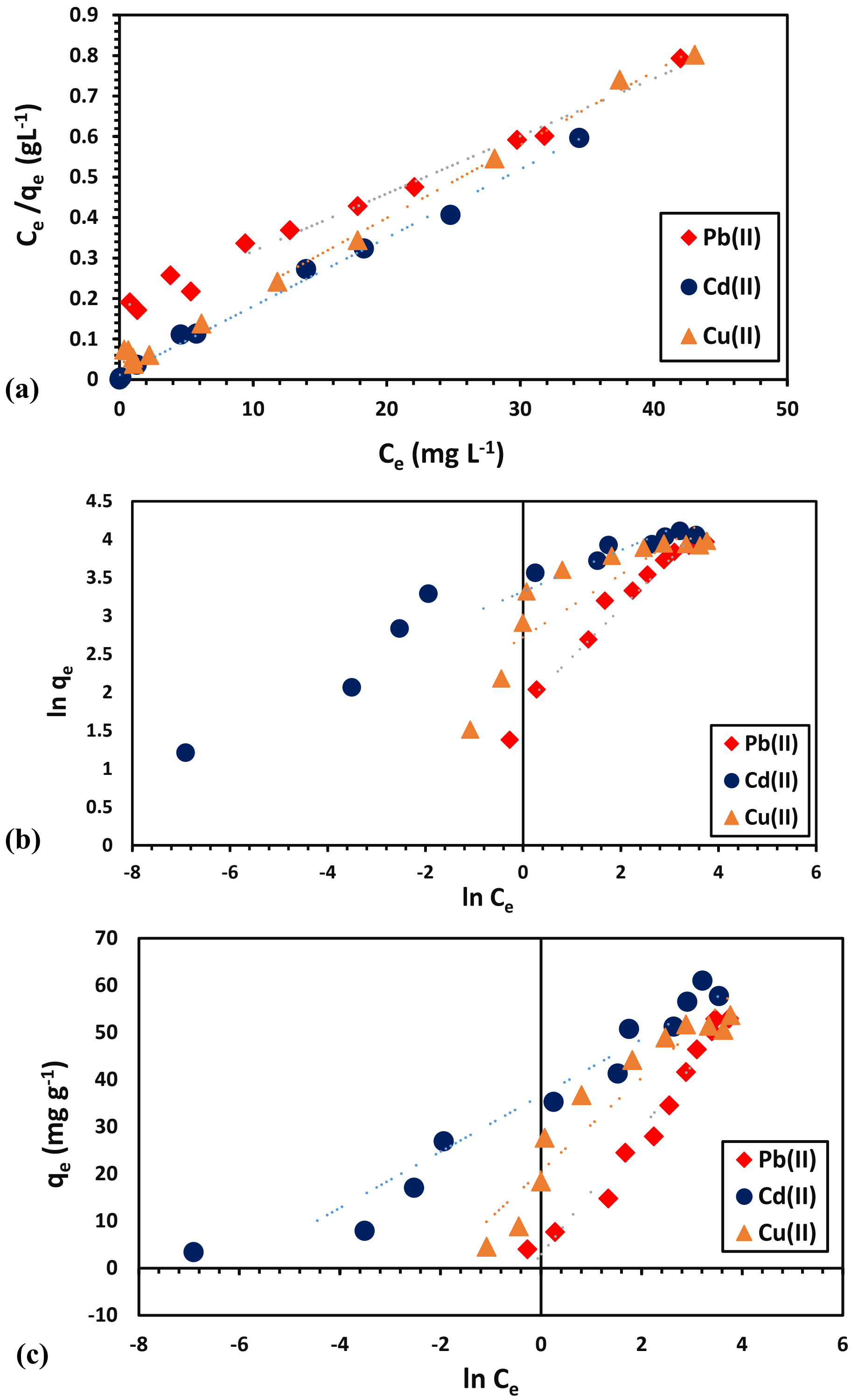

Figure S6: Adsorption isotherm models for the removal of Pb(II), Cd(II), and Cu(II) ions using the prepared adsorbent. (a) Langmuir isotherm model; (b) Freundlich isotherm model; (c) Temkin isotherm model.

References

1 K. Z. Elwakeel, A. Shahat, Z. A. Khan, W. Alshitari and E. Guibal, *Chem. Eng. J.*, 2020, **392**.

2 D. Dong, Y. Li, J. Zhang and X. Hua, *Chemosphere*, 2003, **51**, 369-373.

3 S. Lagergren, *Kungliga Svenska Vetenskapsakademiens Handlingar*, 1898, **24**, 1-39.

4 Y. S. Ho and G. McKay, *Chem. Eng. J.*, 1998, **70**, 115-124.

5 W. J. Weber and J. C. Morris, *J. Sanit. Eng. Div.*, 1963, **89**, 31-60.

6 J. Zeldowitsch, *Acta. Physicochim. URS*, 1934, **1**, 364-449.

7 I. Langmuir, *J. Am. Chem. Soc.*, 1918, **40**, 1361-1402.

8 H. M. F. Freundlich, *Z. Phys. Chem.*, 1906, **57**, 385-470.

9 M. I. Temkin and V. Pyzhev, *Acta Physiochim URSS*, 1940, **12**, 327-356.

10 F. K. Mahar, L. He, K. Wei, M. Mehdi, M. Zhu, J. Gu, K. Zhang, Z. Khatri and I. Kim, *Chemosphere*, 2019, **225**, 360-367.

11 J. Zhang, J. Shao, Q. Jin, X. Zhang, H. Yang, Y. Chen, S. Zhang and H. Chen, *Sci. Total Environ.*, 2020, **716**, 137016.

12 C. S. Nkutha, N. D. Shooto and E. B. Naidoo, *South African Journal of Chemical Engineering*, 2020, **34**, 151-157.

13 L. Xu, C. Chen, J.-B. Huo, X. Chen, J.-C. E. Yang and M.-L. Fu, *Environ. Technol. Innov.*, 2019, **16**, 100504.

14 T. I. Shalaby, M. F. El-Kady, A. E. H. M. Zaki and S. M. El-Kholy, *Water Supply*, 2016, **17**, 176-187.

15 S. Mishra and N. Verma, *Chem. Eng. J.*, 2017, **313**, 1142-1151.

16 Y. Yan, B. Sarkar, L. Zhou, L. Zhang, Q. Li, J. Yang and N. Bolan, *Environ. Pollut.*, 2020, **266**, 115177.

17 R. Soto-Ramírez, M.-G. Lobos, O. Córdova, P. Poirrier and R. Chamy, *J. Hazard. Mater.*, 2021, **411**, 125059.

18 A. Satya, A. Harimawan, G. Sri Haryani, M. A. H. Johir, L. N. Nguyen, L. D. Nghiem, S. Vigneswaran, H. H. Ngo and T. Setiadi, *Environ. Technol. Innov.*, 2021, **21**, 101194.

19 S. R. Korake and P. D. Jadhao, *Heliyon*, 2021, **7**.

20 S. Yang, Z. Huang, C. Li, W. Li, L. Yang and P. Wu, *Colloids Surf. Physicochem. Eng. Aspects*, 2020, **602**, 125171.

21 P. M. Thabede, N. D. Shooto, T. Xaba and E. B. Naidoo, *J. Environ. Chem. Eng.*, 2020, **8**, 104045.

22 S. Tasharrofi, Z. Rouzitalab, D. M. Maklavany, A. Esmaeili, M. Rabieezadeh, M. Askarieh, A. Rashidi and H. Taghdisian, *Sci. Total Environ.*, 2020, **736**, 139570.

23 Y. Taamneh and S. Sharadqah, *Appl. Water Sci.*, 2017, **7**, 2021-2028.

24 M. Claros, J. Kuta, O. El-Dahshan, J. Michalička, Y. P. Jimenez and S. Vallejos, *J. Mol. Liq.*, 2021, **325**, 115203.

25 T. Kamilya, S. Mondal and R. Saha, *Environ. Sci. Pollut. Res.*, 2022, **29**, 20017-20034.

26 Jumina, Y. Priastomo, H. R. Setiawan, Mutmainah, Y. S. Kurniawan and K. Ohto, *J. Environ. Chem. Eng.*, 2020, **8**, 103971.

27 Q.-x. Jing, Y.-y. Wang, L.-y. Chai, C.-j. Tang, X.-d. Huang, H. Guo, W. Wang and W. You, *Trans. Nonferrous Met. Soc. China*, 2018, **28**, 1053-1060.

28 M. Shahrashoub and S. Bakhtiari, *Microporous Mesoporous Mater.*, 2021, **311**, 110692.

29 X. Zheng, N. Yu, X. Wang, Y. Wang, L. Wang, X. Li and X. Hu, *Sci. Rep.*, 2018, **8**, 6463.

30 Y. Chu, M. A. Khan, M. Xia, W. Lei, F. Wang, S. Zhu and X. Yan, *Chem. Eng. Res. Des.*, 2020, **157**, 142-152.
31 A. Saleem, J. Wang, T. Sun, F. Sharaf, M. Haris and S. Lei, *J. Environ. Chem. Eng.*, 2020, **8**, 104430.
32 J. Dong, Y. Du, R. Duyu, Y. Shang, S. Zhang and R. Han, *Bioresour. Technol. Rep.*, 2019, **6**, 96-102.
33 T.-B. Nguyen, T.-B.-C. Ho, C. P. Huang, C.-W. Chen, W.-H. Chen, S. Hsieh, S.-L. Hsieh and C.-D. Dong, *Chemosphere*, 2022, **304**, 135276.
34 A. E. Martell and R. M. Smith, *Critical stability constants*, Springer, 1974.
35 W. Quiroz, *ChemTexts*, 2021, **7**, 7.